

Preparation and Magnetic Properties of Nanosize Fe-Co-Ni Alloy and Composite Particles by Water-in-Oil Microemulsions

ZHANG Chao-ping, LEI Bing-xin, LI Zhen

(Department of Chemistry, Guizhou University, Guiyang 550025, China)

Abstract: A well-mixed Fe-Co-Ni alloy and composite nanoparticles were successfully prepared by chemical reduction of the corresponding metal ions with KBH_4 in the microemulsion system of water/ Span-80/ *n*-butanol/*n*-heptane. Crystalline structure, phase transformation properties of the synthesized materials were investigated using X-ray diffraction (XRD), thermogravimetry (TG) and differential scanning calorimeter (DSC). Effects of the processing parameters on the alloying composition, phase transformation and morphologic character were analyzed by using a combination of transmission electron microscope (TEM), energy dispersive X-ray spectrometry (EDS), atomic force microscope (AFM), and electron diffraction (ED), which suggest the Fe-Co-Ni alloying will form a structure in the ternary metal composite nanoparticles. The magnetic property was investigated by using toric AC magnetic field. The results indicated that the configurations of Fe-Co-Ni alloys and composite are pine needle and hummock shapes and Fe-Co-Ni nanoparticles are 150 nm in length and 20–30 nm in diameter, annealed at 150–400 °C respectively. The susceptibilities decreased with the increase of the calcining heat. In all heating experiments several exothermic processes were detected that are related to the crystallization of the amorphous-like alloy and composite. The possible formation mechanism of Fe-Ni-Co alloy and composite nanoparticles was discussed.

Keywords: Fe-Co-Ni alloy; composite; nanoparticles; microemulsions; TG/DSC

W/O 微乳液法制备 Fe-Co-Ni 合金和复合物 纳米颗粒材料及其磁性能研究

张朝平, 雷炳新, 李 振

(贵州大学化学系, 贵阳 550025)

摘要: 在水/司班-80/正丁醇/正庚烷组成的微乳液系统中,用 KBH_4 还原相应的金属离子成功地制备了 Fe-Co-Ni 合金纳米质点. Fe-Co-Ni 合金和复合物纳米微粒的晶体结构、相变性质用 X 射线衍射(XRD)、热重分析(TG)和示差扫描量热仪(DSC)作了考察. 过程参数对合金和复合物组成、相变以及形态特征的影响用透射电子显微镜(TEM)、X 射线能量散射谱(EDS)、原子力显微镜(AFM)和电子衍射(ED)进行了分析,结果表明 Fe-Co-Ni 的合金化将形成三元金属复合物纳米结构. 合金的磁性质用环形 AC 磁场作了研究. 结果表明,Fe-Co-Ni 合金和三元金属复合物纳米质点当其在 150~400 °C 退火后,呈现松针和山丘状,其长度和直径分别为 150 nm 和 20~30 nm. 磁感应性随煅烧温度的增加而降低; 在所有的热分析实验中检测到几个放热过程对应于无定形合金的晶化. 对形成

收稿日期: 2011-04-12.

基金项目: 贵州省省长基金资助项目(2008(101)).

作者简介: 张朝平(1941—),男,教授.

通讯作者: 张朝平, cpingzhang@163.com.

Fe-Co-Ni 合金和金属复合物的可能机理作了讨论。

关键词: Fe-Co-Ni 合金; 复合物; 纳米质点; 微乳液; TG/DSC

中图分类号: O648.2; TQ138.1

文献标志码: A

文章编号: 1672-6030(2012)01-0036-010

Ternary Fe-Co-Ni alloys and composites have been extensively studied as soft magnetic materials due to their superior properties relative to binary Fe-Ni alloys and composites as write head core materials in hard-disk-drives^[1-3]. With increasing storage density requirements, there is a need for recording heads to write on high-coercivity media at high frequencies, which has raised new requirements for the write-head material that cannot be met by Ni₈₀Fe₂₀^[4]. Therefore, new soft magnetic materials with higher saturation magnetizations (1 T) such as Co-Fe alloys, Co-Fe-Ni alloys and other Co-Fe based alloys have been developed^[5-11]. Monodisperse Co-Ni and Fe-Co-Ni composite materials have fine magnetic resonance^[7]. The substitution of small amounts of Co or Ni for Fe in Fe-based magnetic materials generally results in an increase of saturation magnetization^[12]. Mechanical alloying (MA) allows producing alloys in large quantities but the process induces impurities in the milled powders^[13]. There is a great interest in developing nanomaterials with complicated architectures, e. g., nanoparticles and nanowires, due to their unusual physico-chemical properties arising from the quantum effects^[14-15]. In general, materials with nanostructures in high aspect ratios can be successfully prepared by the employment of templates (including membranes and surfactants) as “molds”^[16-19]. But the report for preparation of Fe-Co-Ni alloys and composites nanoparticles by using the W/O microemulsions is absent at the same time. In this paper, the preparation of a nanocrystalline (Fe, Co, Ni) alloy and composite in W/O microemulsions of water/Span-80/*n*-butanol/*n*-heptane by using reduction either of Fe²⁺, Co²⁺ and Ni²⁺ ions using the KBH₄ is reported. The X-ray diffraction (XRD), transmission electron microscope (TEM), atomic force microscope (AFM), electron diffraction (ED), and thermogravimetry (TG) / differential scanning calorimeter (DSC) were used to characterize the crystalline structure, phase transformation properties of the synthesized Fe-Co-Ni alloys and composites as well as size and composition distribution of the resultant nanoparticles, which suggests the Fe-Co-Ni alloying will form a structure in the ternary metal composites nanoparticles.

TEM and AFM characterizations indicated the presence of pine needle and hummock shape in the alloys and composites.

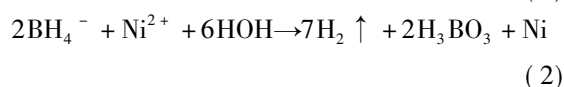
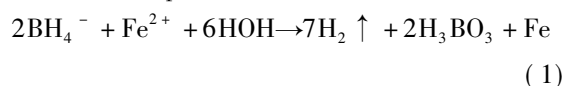
1 Experiment

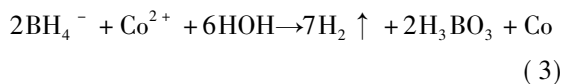
1.1 Materials and methods

All chemicals including Span-80 (sorbitan monooleate), FeSO₄·7H₂O, CoCl₂·6H₂O, NiCl₂·6H₂O, NaOH, potassium borohydride, *n*-butanol, and *n*-heptane used were of analytical grade and purchased from Chemical Reagents Corporation. Water used in the experiments was deionized (DI).

1.2 Preparation of Fe-Co-Ni alloy and composite nanoparticles

The microemulsion system used in this study consists of Span-80 as a surfactant, *n*-butanol as a co-surfactant, *n*-heptane as the continuous oil phase, and both the Fe²⁺, Co²⁺ and Ni²⁺ precursor solution and potassium borohydride as the dispersed aqueous phase. The aqueous phases in two microemulsion systems have the same volume fraction but with different compositions as indicated in Tab. 1. The aqueous phase in microemulsion II contained KBH₄ as the reducing agent. The amount of KBH₄ was in stoichiometric excess compared with the equivalent of Fe²⁺, Co²⁺ and Ni²⁺ precursor solution in microemulsion I. The two microemulsions were prepared separately by mixing with 3% surfactant, 60% *n*-butanol, 30% *n*-heptane, and 7% of the aqueous phase. A small amount of additional *n*-butanol was then titrated slowly into each of the microemulsion system with stirring until the microemulsion system turned transparent. The two stable microemulsions were then mixed with a stirrer at (25 ± 0.5) °C. The Fe-Co-Ni nanoparticles were formed upon contact between the precursor containing droplets and potassium borohydride containing droplets. The reduction reactions could be expressed as





The black powder product was collected in a filter paper and washed with absolute ethanol and deionized water to remove the impurities. It was rinsed with pure acetone to remove water and then dried at 60 °C in air. Sample was also heated under an atmosphere environment in the range of 250—450 °C about 40 min. A series of samples were prepared, when changing the radius of water core ($w = c(\text{H}_2\text{O}) / c(\text{Span-80})$), the method of addition of FeSO_4 , CoCl_2 and NiCl_2 , or the mole ratio of $\text{FeSO}_4 / \text{CoCl}_2 / \text{NiCl}_2$ in the initial precursor solution respectively during the other conditions are the same as those in Tab. 1.

Tab. 1 Compositions of microemulsion system used for synthesis of Fe-Co-Ni nanoparticles

Compositions	Microemulsion I	Microemulsion II	$\varphi / \%$
Aqueous phase	$\text{FeSO}_4 + \text{CoCl}_2 + \text{NiCl}_2$	Borohydride potassium	7
Surfactant	Span-80	Span-80	3
Co-surfactant	<i>n</i> -butanol	<i>n</i> -butanol	60
Oil phase	<i>n</i> -heptanes	<i>n</i> -heptane	30

1.3 Characterization of Fe-Co-Ni nanoparticles

The crystalline structure was examined by an XRD (Rigaku Co. Model DLMAX-2200) with Cu-K α radiation ($\lambda = 0.154\ 05\ \text{nm}$). The microstructures and morphologies of nanoparticles were characterized using a JEM-2000FXII (Japan) TEM measurement. The particles composition was determined using energy dispersive X-ray spectrometry(EDS) by measuring characteristic X-rays from areas approximately $300\ \mu\text{m} \times 300\ \mu\text{m}$ in size from the upper, central, and lower part of each nanoparticle. These values were then averaged. The susceptibility of Fe-Co-Ni nanoparticles was performed at room temperature by using toric AC magnetic field (FM-A, Fudan University, China). TG/DSC analyses were performed using a NETZSCH STA 409(Germany); samples of approximately 5 mg were heated in pure nitrogen from 0 to 1 000 °C, at a rate of 5 °C/min. The roughness and surface morphology were characterized by using an AFM (CSPM-3100 Ban-Yuan Nano-Co, China) measurement.

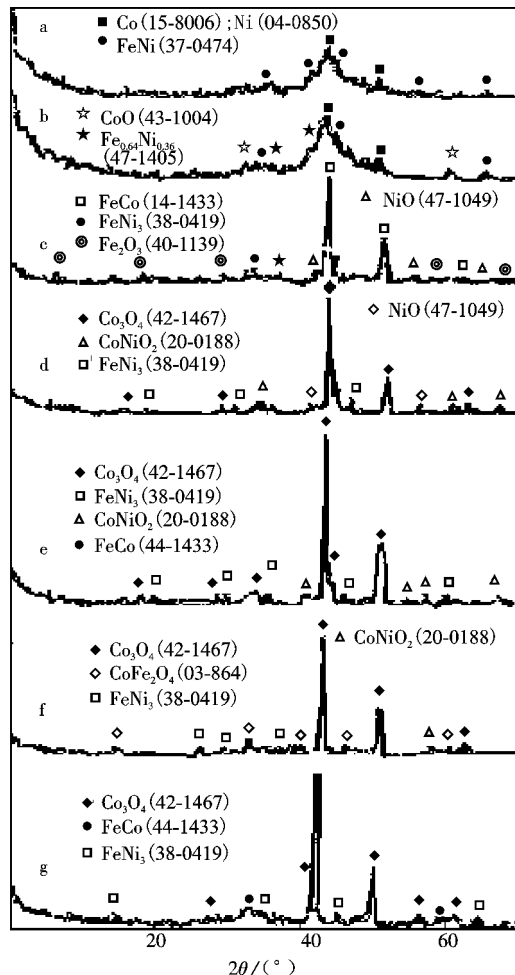
2 Results and discussion

2.1 XRD and TEM investigations for the samples

XRD experiments were carried out in order to identify

the major phases present in the alloys and composites after the ageing treatment. Fig. 1 shows the XRD patterns of the Fe-Co-Ni nanoparticles using microemulsion process under different temperatures for 40 min. There may be a doubt that the alloys and composites with various nanostructures are metals, alloys or oxides. Accordingly, the crystalline information of the nanoparticles and nanoclusters prepared in this work has obtained from the grazing incidence XRD patterns and TEM images. Typical results for the alloys and composites are shown in a—g of Fig. 1, respectively. On pattern a and b, diffraction peaks corresponding to elements Co, Ni and FeCo or Fe-Ni alloys are clearly found, revealing the fact that the nanoparticles formed under 150 °C in a of Fig. 1 is metallic, at least, consisting of two alloys. Moreover, the crystalline quality of $\text{Fe}_{0.64}\text{Ni}_{0.36}$ should be better than that of FeCo because of the narrower peak width and higher diffraction intensity for the former alloy. The similar diffraction peaks are also found on pattern c—g, in which the relative intensities correspond to FeNi_3 and FeCo, and oxides (especially is Co_3O_4) peaks are increased in comparison with those on patterns a and b. The results suggest that FeNi_3 and FeCo alloys and Co_3O_4 are the main crystalline components of the nanoparticles. In addition, some secondary peaks corresponding to the CoNiO_2 or NiO, CoO and CoFe_2O_4 were found, which suggests the formation of certain composite oxides species in the nanoparticles. In fact, the presence of composite oxides within the Fe-Co-Ni alloys is usually found in the iron-group alloys since Ni and Co oxides can be easily prepared by different methods^[20-23]. The oxidation behaviors of the ternary nanoparticles and the phase components after oxidation are similar to those of the binary nanoparticles^[24]. The average diameters and lattice constants (see Tab. 2) corresponding to the different heat-treated were calculated from their respective XRD spectra by the Scherrer expressions ($D = 57.3k\lambda / \beta \cos \theta$) and Bragg equation ($l/2d = h^2/a^2 + k^2/b^2 + l^2/c^2$ and $2d \sin \theta = n\lambda$). From Tab. 2, it is evident that the average diameter and lattice constant of the prepared Fe-Co-Ni samples increase with the calcining heat increasing. This is attributed to the calcinations Fe-Co-Ni alloy particles expansion in the ultra-fine particles^[25] and oxidation of reduced Fe, Co, and Ni particles

in microemulsion^[7,26]. The diffraction peak positions in c of Fig. 1 of the (111) and (200) planes are corresponding to 2θ of 44.28° and 51.6° respectively. $\sin^2 22.14^\circ / \sin^2 25.8^\circ$ equals to 3:4, which indicates that Fe-Co-Ni alloy nanoparticles are the face-centered cubic structures. The ratio of the square of the radius for the concentric rings is 3:4:8:11:12 in this electron diffraction pattern (see Fig. 2(b)).

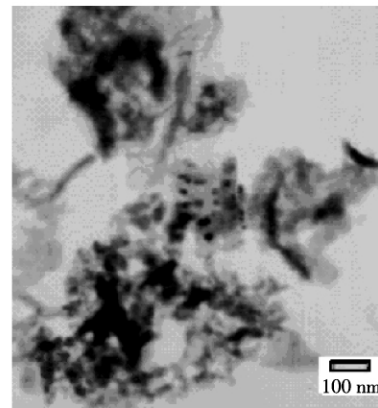


a—Not annealed; b—150 °C; c—250 °C; d—300 °C; e—350 °C; f—400 °C; g—450 °C

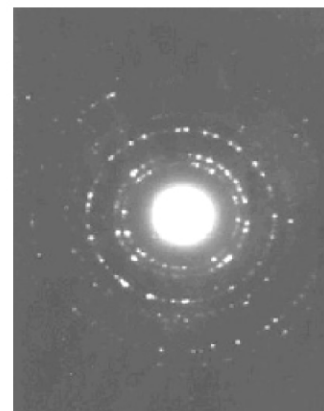
Fig. 1 XRD patterns of Fe-Co-Ni alloy nanoparticles under different temperatures for 40 min

Tab. 2 Average diameter and lattice constant of the prepared Fe-Co-Ni samples at annealed

Calcinations/°C	Average diameter/nm	Lattice constant/nm
250	8.58	0.353 01
300	16.67	0.353 10
350	16.90	0.353 10
400	17.70	0.354 01
450	18.88	0.354 31



(a) TEM of the sample calcined at 250 °C for 40 min



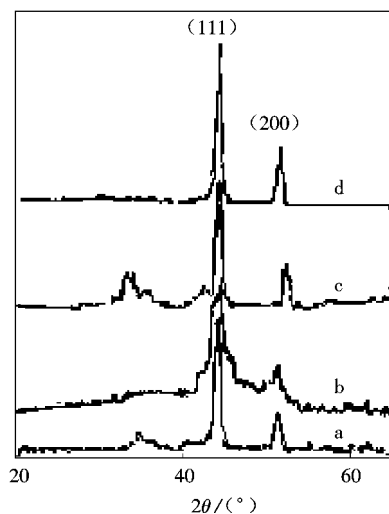
(b) Electron diffraction pattern of a region

Fig. 2 TEM of the sample calcined at 250 °C for 40 min and electron diffraction pattern of a region

The predominant morphology of TEM image of the sample calcined at 250 °C, as shown in Fig. 2(a), which indicates nanorods with average length of about 150 nm and diameter of 20—30 nm exist and there are some nanospheres with the diameter of about 25 nm. The selected area electron diffraction (SAED) pattern of the alloys and composites carried out on one single particle showed diffraction rings with spots superimposed (Fig. 2(b)), which suggests that the formed nanoparticles are polycrystalline.

The influence of the metal ions concentrations on the particles sizes indicates that the lower nickel ions are useful for preparing tinier particles. Lower iron ions, more nickel and cobalt atoms were reduced and absorbed on the nuclei, and then they aggregated into larger spherical particles as demonstrated by XRD in Fig. 3 and Tab. 3 and average diameter was calculated using Scherrer

equation respectively. According to EDS (see Fig. 4) analysis, the compositions of Fe, Co and Ni in different individual regions are not in close and have a little deviation. The peak of copper is sometimes present on the EDS spectra due to the specimen holder.



a— $n_{Fe}:n_{Co}:n_{Ni}=2:4:4$; b— $n_{Fe}:n_{Co}:n_{Ni}=2:2:6$;
c— $n_{Fe}:n_{Co}:n_{Ni}=2:6:2$; d— $n_{Fe}:n_{Co}:n_{Ni}=1:4.5:4.5$

Fig. 3 XRD of Fe-Co-Ni alloys prepared for different reactant ratios

Tab. 3 Average size and lattice constant of Fe-Co-Ni alloys prepared according to reactant ratio

$n_{Fe}:n_{Co}:n_{Ni}$	Average diameter/ nm	Lattice constant/nm
2: 4: 4	14. 15	0. 354
2: 2: 6	5. 25	0. 353
2: 6: 2	12. 87	0. 354
1: 4. 5: 4. 5	21. 77	0. 354

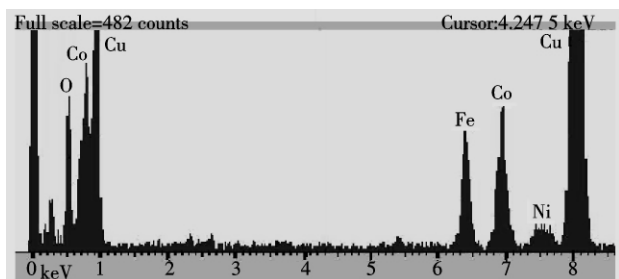
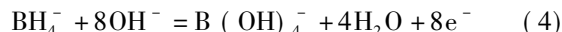


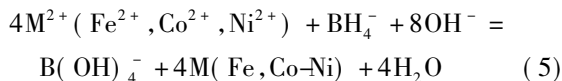
Fig. 4 EDS spectra of sample annealed at 250 °C for 40 min

A possible mechanism of formation of the Fe-Co-Ni nanoparticles may be as follows.

The normal potential of BH_4^- is -1.24 V , which can give out 8 electrons in alkaline medium^[27]



The normal potentials of Fe^{2+} , Co^{2+} , and Ni^{2+} are -0.877 V , -0.73 V and -0.72 V (alkaline medium) respectively, then we can get



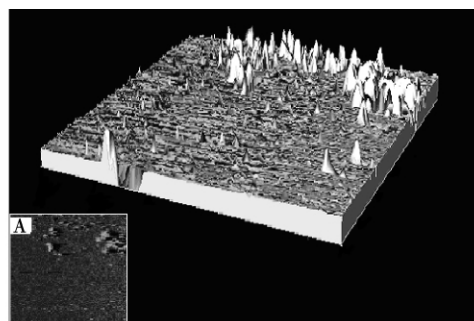
At the beginning, $Fe(OH)_2$, $Co(OH)_2$, and $Ni(OH)_2$ suspension was formed by the reaction of Fe^{2+} , Co^{2+} , Ni^{2+} and OH^- . The strong alkalinity of the solution resulted in $Fe(OH)_2$, $Co(OH)_2$, and $Ni(OH)_2$ which all have negative charge. Withal, NaOH is added to the polyol which will increase the monodispersity of the nanoparticles and, also will accelerate the chemical reactions. So the $Fe(OH)_2$, $Co(OH)_2$, and $Ni(OH)_2$ interdiffuse with the surfactant Span-80, to form Span-80- $Fe(OH)_2$, $Co(OH)_2$, and $Ni(OH)_2$ mutualism^[28]. It seemed that Span-80 wrapped the tiny particles and became spherical micelles. Therefore, the alloys nucleated at the micelles by reduction with potassium borohydride. While the *n*-heptane was added in the system, layer micelles may be formed with *n*-heptane in the layers like sandwich. So the alloys nucleated at the layer composed by Span-80- $Fe(OH)_2$, $Co(OH)_2$, and $Ni(OH)_2$. The nanosheet was obtained, then the 2D nanosheets rolled into nanorods^[29], for which the driven force can be attributed to the decrease of the surface free energy. Part of the non-ionized surfactant Span-80 may form chainlike structure due to the assembly in water. Then, some 1D liquid reaction fields could be formed in the Span-80 and water mixed system^[30], which may result in the formation of Fe-Co-Ni rods as shown in Fig. 2(a).

The synthesis of nanoparticles in microemulsions allows one to obtain monodisperse size of the particles and in some cases to control the size and shape of the particles by variation of the size of the microemulsion droplet radius and of the precursors concentrations. Two models are proposed for the formation of the particles: the first is based on the LaMer diagram^[31], and the second is based on the thermodynamic stabilization of the particles. In the first case, the particle size and shape varies as a function of either the size of the inner water cores or the precursor concentration; in the second case, the particle size is independent of these parameters^[32]. To form a stable nucleus, a minimum number of atoms are required. Thus, for nucleation several atoms must collide at the same

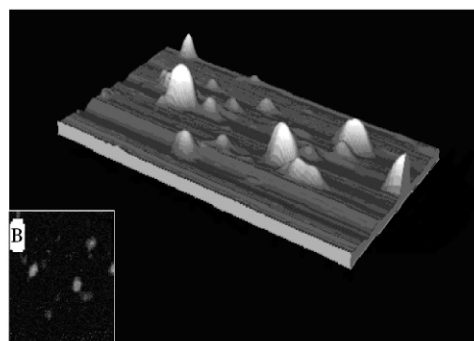
time, and the probability of this phenomenon is much lower than the probability of collision between a single atom and an already formed nucleus. The latter phenomenon is called the growth process. At the very beginning of the reduction, nucleation occurs only in water cores that contain enough ions to form a nucleus. At this moment, the micellar aggregates act as “reaction cages” where the nuclei are formed. On the other hand, the microemulsion being dynamic, the water cores rapidly rearrange. The other ions brought into contact with the existing nuclei essentially participate in their growth process^[33].

2.2 AFM observation

The results of AFM observation of individual Fe-Co-Ni alloy and composite nanoparticles were shown in Fig. 5. The crystal surface morphologies of pine needle and hummock shapes were found. The hummocks are separated well from each other, whose surface is slippery and has no further microstructure. The three-dimensional and planar views of Fe-Co-Ni nanoparticles in different annealed and scan sizes are shown in Fig. 5(a) and Fig. 5(b) respectively. Fig. 5 shows a typical AFM image of the surface morphology whose scan size is $28 \mu\text{m} \times 28 \mu\text{m}$



(a) AFM image of three-dimensional and profile in different scan sizes for the 150 °C/40 min annealed (Scan size: $28 \mu\text{m} \times 28 \mu\text{m}$)



(b) AFM image of three-dimensional and profile in different scan sizes for the 350 °C/40 min annealed (Scan size: $1.0 \mu\text{m} \times 0.57 \mu\text{m}$)

Fig. 5 AFM images for three-dimensional and profiles in different scan sizes

μm . One (part A of Fig. 5) was relatively thickness with average area of $(4.96 \pm 0005) \text{ nm}^2$ and average dimension of about 249 nm, grain sum of 3 853, and the other (part B of Fig. 5) showed that these particles were hummock shape at the scan size (average area of $(1.94 \pm 0006) \text{ nm}^2$, average dimension of 397 nm, grain sum of 122. Looking at different points for the 150 °C/40 min and 350 °C/40 min annealed surface, it is found that the average height of the particles is approximately 3.31 nm and 6.86 nm respectively. As can be seen, the distribution of particles is not uniform. AFM images in Fig. 5 show that the Fe-Co-Ni nanoparticles are continuously flat after annealed and those subsequent heat treatments roughen the particles surface. As the annealing temperature increases, the surface roughness also increases. Fig. 6 plots the surface roughness as a function of temperature. The results show that there is no significant change in nanoparticles morphology below 150 °C, although we cannot exclude atomic scale events on the surfaces. The change in surface roughness is small up to 150 °C, where upon it starts to increase. A roughening transition occurs somewhere between 250 °C and 450 °C, where surface roughness increases dramatically. Thus, the Fe-Co-Ni nanoparticles begin cluster forming at temperature somewhere between 250 °C and 450 °C, and complete the process above 450 °C. DSC shows that the early stage of phase separation occurs at around 150 °C, at which stage no obvious surface morphology change is observed.

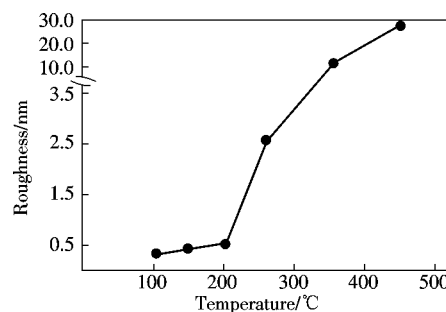


Fig. 6 Surface roughness as a function of temperature

2.3 Thermal stability of Fe-Ni-Co nanoparticles

DSC measurements performed supported the existence of an amorphous phase deduced from XRD and TEM. Phase transformation of powders was studied by using TG/DSC measurements. Fig. 7 shows the sample

crystallizes in a complex three-stage crystallization process. The calorimetric data reveal a broad hump in the temperature range of 35—100 °C, and an apparent 1.48% weight loss in the TG curve, which began at about 35 °C, and it was associated with the loss of absorption water and crystalline water. From 100 to 288.9 °C, it showed 3.52% total losses in TG curve. It is due to decomposition of the ethanol which is used as a washing agent and other organic agent as well as copolymer part of the material. In all heating experiments several exothermic processes were detected that are related to the crystallization of the amorphous-like alloy. There are at least three processes for samples of Fe-Co-Ni powders. The first crystallization peak starts at about 243.2 °C and the second at about 416.8 °C. The crystallization process in the rapidly solidified samples produces a very sharp main exothermic peak and at least one flat high temperature third peak at about 572.9 °C. The values obtained can reasonably be associated with a nucleation and grain growth process as in the cases of the Co-based and Ni-based nanoparticles^[34]. In the Fe-based alloy, oxides have several kinds of structures such as FeO, Fe₃O₄ and

Fe₂O₃. The three peaks illustrate the oxidization of the sample through three stages. The thermal stability of the Co- and Ni-based nanoparticles is slightly higher than that of the Fe-based. On the basis of our results, it can be suggested that these nanoparticles are stable and secure below 200 °C in air. Note that, the peak position of mass derivative (TG curve) is the same compared to the exothermic peak obtained from the DSC curve. Fig. 7 shows the TG and DSC curves of a representative sample. All synthesized show analogous, well-defined TG/DSC peaks. Finally, the amount of unstable substance in all the samples is lower (about 4.16%) based on the weight loss at low temperatures (35—200 °C) of the TG diagram^[35-36]. It can be seen from Fig. 7 that there is an apparent 14.66% weight increase from about 288.9 °C to 700 °C. The reaction occurring in the above process could be written as

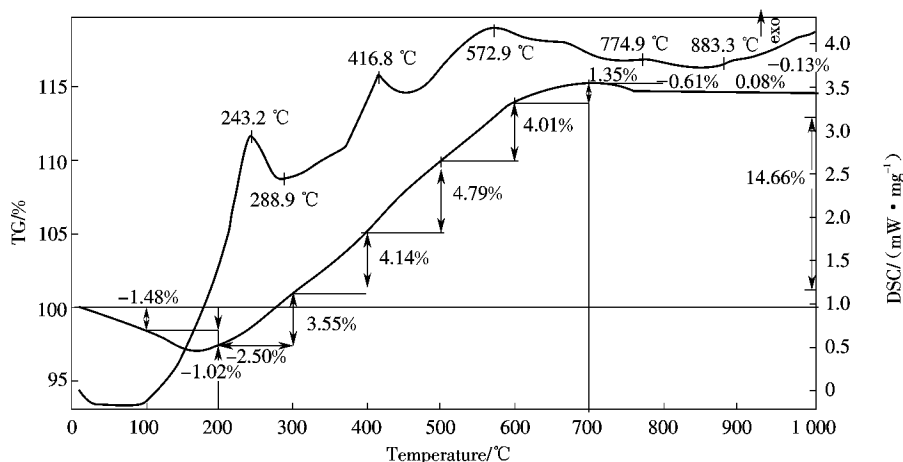
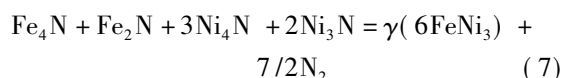
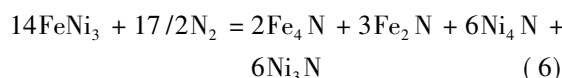


Fig. 7 TG/DSC curve of Fe-Co-Ni sample

At first, the Fe-Ni-Co alloy reacted with the adsorbed N₂ species, resulting in the formation of Fe₄N + Fe₂N and Ni₄N + Ni₃N respectively; when Fe-Ni-Co was fully consumed and the fcc nitride Fe₄N (γ) has a narrow range of homogeneity around 20% N. The cph nitride Fe₂N (ε) has a broad composition range from 15% N to at least 33% N^[37]. The N-Ni phase diagram is only partially known. The Ni-rich intermediate phases are Ni₄N

and Ni₃N^[37]. The ordered Fe-Ni is the only intermediate phase in the system. Then it will translate into γ(Fe, Ni) alloys when the temperature exceeds 800 °C^[38]. The nitrogen in Fe₄N, Fe₂N and Ni₄N, Ni₃N will be removed and Fe-Ni alloy will be formed again, and the results correspond with their phase diagram^[38]. With regard to the structural characteristics of 3 d transition metal nitrides, it can be recognized that the larger metal atoms constitute

the fundamental structure and the smaller nitrogen atoms are located at interstitial sites^[39]. Generally, stoichiometric compounds of metal nitrides are not always obtained, because the metal nitrogen system gives the interstitial compounds. Co-N films were also prepared^[40] by reactive sputtering. They are reported to consist of two phases: a hcp Co and a Co nitride phase. In particular, a Co₄N phase was identified with a fcc structure made up of Co atoms with a nitrogen atom at the center of each cubic unit cell.

2.4 Magnetic properties of Fe-Ni-Co alloys and composites

The magnetic properties of Fe-Co-Ni alloys nanoparticles were analyzed by the toric AC magnetic field. Fig. 8 shows the susceptiveness curves of the samples. It can be seen that susceptiveness of Fe-Co and Ni alloy nanoparticles decreases with elevation of sintered at room temperature. The values of susceptiveness indicate the effect of heat treatments of the investigated powder on precursor which transformed from an amorphous state with preferable magnetic induction. But the intermetallic Fe-Co-Ni at 150—400 °C has lower magnetic induction. On the other hand, from the values of susceptiveness χ_m in Fig. 8 in case of the powder itself, the susceptiveness has higher values than the heat treated and also the sintered one, because the powdered form has a very fine structure, having a single domain structure with higher susceptiveness values than the consolidated one which has a strong particle-particle interaction decreasing the susceptiveness. The susceptiveness χ_m value decreased with the sintered increasing. The origin of this behavior may be found in the competition among different changes occurring in the

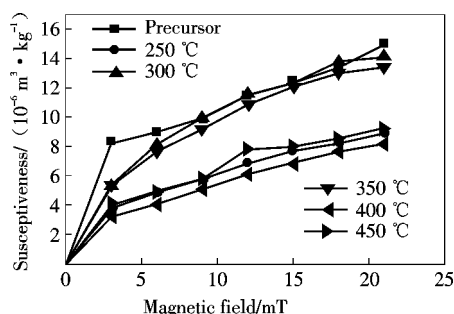


Fig. 8 χ_m in dependence on the magnetic field at room temperature for the Fe-Co-Ni nanoparticles under different heat treatments

evolution of the structure. Likely, at the beginning of sintering, a small grain size and poor homogeneity of Fe-Co-Ni alloy, besides the presence of metal nitrides(see Section 2.3) are observed; while at higher temperatures and upon increasing the sintering time, grain growth and Fe-Co-Ni inner diffusion are responsible for the decrease of χ_m . Furthermore, the addition of nitrogen is reported to progressively reduce the saturation magnetization of Co. The results of the literature, therefore, indicate that N can enter solid solution, the Co-Ni alloy, but has an adverse effect on the magnetic properties^[40].

3 Conclusion

Synthesis of alloys containing Fe-Co-Ni nanoparticles has been carried out successfully by a W/O microemulsion of water/ Span-80/*n*-butanol/*n*-heptane route. It has been shown that mixing of iron with cobalt and nickel ions in the presence of KBH₄ leads to the formation of nanoscale alloy particles when calcined within the temperature range of 250—450 °C. The structural and composition distribution of the resultant nanoparticles of Fe-Co-Ni alloy were performed by means of XRD, TEM, AFM, ED and TG/DSC analysis. The analysis of typical Fe-Co-Ni particles diameters indicates an average 150 nm in length and 20—30 nm in diameter. The Fe-Co-Ni nanoparticles show some degree of the crystallization. The grains formed initially grow with the increase of the annealing temperature, indicating a large number of grains in the shape of equally sized pine needle shape and hummock grains that are observed in individual clusters. All DSC scans show several reactions on heating. At low temperature, about 243 °C, the exothermal process detected is associated to structural relaxation, which is related to the crystallization of the amorphous-like alloy and composite. The size of Fe-Co-Ni nanoparticles depends on annealing, which increases with the rise of annealing temperature.

Acknowledgments

The author wants to thank Prof. Gong Guohong and Liu Shirong for carrying out the XRD and TEM measurements and the Gov. of Guizhou Province for financial support.

References:

- [1] Osaka T, Asahi T, Yokoshima T. Electroless-deposited soft

- magnetic underlayer on silicon disk substrate for double-layered perpendicular magnetic recording media [J]. *J Magn Mater*, 2005, 287: 292-297.
- [2] Yoshino M, Kikuchi Y, Sugiyama A, et al. Preparation of high magnetic flux density CoNiFeB film by electroless deposition for application to magnetic recording devices [J]. *Electrochimica Acta*, 2007, 53 (2): 285-289.
- [3] Zhou Debi, Tu Saiqi, Ren Zhiwei, et al. Microemulsion synthesis and characterization of Fe-Co-Ni alloy nanoparticles [J]. *J Cent South Univ: Science and Technology*, 2007, 35 (4): 706-710.
- [4] Andricacos P C, Robertson N. Future directions in electroplated materials for thin-film recording heads [J]. *J Research and Development*, 1998, 42(5): 671-680.
- [5] Osaka T, Yokoshima T. Corrosion properties of high-performance CoNiFe based soft magnetic thin films prepared by electro or electroless depositions [J]. *Corrosion Engineering Science and Technology*, 2004, 39(1): 38-44.
- [6] Zhang Y, Ivey D G. Electroplating of gold-tin alloys from a sulfite-citrate bath [J]. *Plating and Surface Finishing*, 2004, 91(2): 28-33.
- [7] Mercier D, Levy J C S, Viau G, et al. Magnetic resonance in spherical Co-Ni and Fe-Co-Ni particles [J]. *Physical Review B*, 2000, 62(1): 532-544.
- [8] Liu X, Miyao T, Fu Y, et al. Soft magnetic properties of Fe-Co films with Co underlayer [J]. *J Magn Mater*, 2006, 303(2): e201-e204.
- [9] Lee K E, Ha N D, Sun D S, et al. Microstructure and soft magnetic properties of CoFeZrO thin films [J]. *J Magn Mater*, 2006, 304(1): e192-e194.
- [10] Xu Baolong, Sun Haiyan, Du Youwei. Fabrication and magnetic properties of cobalt ferrite nanotube arrays [J]. *Nanotechnology and Precision Engineering*, 2011, 9(2): 95-99.
- [11] Yu Changlin, Wen Herui, Yu J C. Preparation of different magnetic Fe₃O₄ nano-crystals under mild conditions with different poly (ethylene glycol) [J]. *Nanotechnology and Precision Engineering*, 2010, 8(2): 161-166.
- [12] Bonastre J, Escoda L, González A, et al. Influence of Ni content on Fe-Nb-B alloy formation [J]. *J Thermal Analysis and Calorimetry*, 2007, 88(1): 83-86.
- [13] González A, Bonastre J, Escoda L, et al. Thermal analysis of Fe (Co, Ni) based alloys prepared by mechanical alloying [J]. *J Thermal Analysis and Calorimetry*, 2007, 87(1): 255-258.
- [14] Bachmann K J. The materials science of microelectronics [J]. *J Am Chem Soc*, 1996, 118(43): 10678-10678.
- [15] Parsons A, Petrashov V T, Sosnin I A. Anomalies in quantum and classical magnetoresistance of semi-metallic nanowires [J]. *Physica B: Condensed Matter*, 2000, 284/285/286/287/288 (2): 1744-1745.
- [16] Hoepfener S, Maoz R, Cohen S R, et al. Metal nanoparticles, nanowires, and contact electrodes self-assembled on patterned monolayer templates: A bottom-up chemical approach [J]. *Advanced Materials*, 2002, 14(15): 1036-1041.
- [17] Lu Gewu, Li Chun, Shi Gaoquan. Synthesis and characterization of 3D dendritic gold nanostructures and their use as substrates for surface-enhanced Raman scattering [J]. *Chemistry of Materials*, 2007, 19(14): 3433-3440.
- [18] Schonenberger C, van der Zande B M I, Fokkink L G J, et al. Template synthesis of nanowires in porous polycarbonate membranes: Electrochemistry and morphology [J]. *J Phys Chem B*, 1997, 101: 5497-5505.
- [19] Zhu J H, Geng S J, Ballard D A. Evaluation of several low thermal expansion Fe-Co-Ni alloys as interconnect for reduced-temperature solid oxide fuel cell [J]. *International Journal of Hydrogen Energy*, 2007, 32(16): 3682-3688.
- [20] Li Xingguo, Takahashi S. Synthesis and magnetic properties of Fe-Co-Ni nanoparticles by hydrogen plasma-metal reaction [J]. *J Magn Mater*, 2000, 214(3): 195-203.
- [21] Wei Xianwen, Zhu Guoxing, Zhou Juhong, et al. Solution phase reduction to Fe-Ni alloy nanostructures with tunable shape and size [J]. *Mater Chem Phys*, 2006, 100(2/3): 481-485.
- [22] Verduzco J A, Betancourt I, Ortiz N, et al. Electric and magnetic properties of Fe-Ni powders-polymeric matrix composites [J]. *Materials Letters*, 2006, 60(1): 2033-2037.
- [23] Bai A, Hu Chichang. Cyclic voltammetric deposition of nanostructured iron-group alloys in high-aspect ratios without using templates [J]. *Electrochem Communications*, 2003, 5(8): 619-624.
- [24] Mathur R, Sharma D R, Vadera S R, et al. Synthesis of nanocomposites of Ni-Zn ferrite in aniline formaldehyde copolymer and studies on their pyrolysis products [J]. *J Alloys and Compounds*, 2003, 358(1/2): 193-204.
- [25] Baranowski B. A simplified quantitative approach to the isothermal hysteresis in metallic hydrides with coherent interphases [J]. *J Alloys and Compounds*, 1993, 200(1/2): 87-92.
- [26] Zhu Junjiang, Xiao Dehai, Li Jing, et al. Characterization of FeNi₃ alloy in Fe-Ni-O system synthesized by citric acid combustion method [J]. *Scripta Materialia*, 2006, 54: 109-113.
- [27] Jiang Xiaoxia, Shen Wei. *Theory and Practice on Chemical Plating* [M]. Beijing: National Defence Industry Press, 2000.
- [28] Luo Fang, Wu Di, Gao Lei, et al. Shape-controlled synthesis of Cu₂O nanocrystals assisted by triton X-400 [J]. *J Cryst*

- tal Growth*, 2005, 285(4): 534-540.
- [29] Porras M, Solans C, Gonzalez C, et al. Studies of formation of W/O nano-emulsions [J]. *Colloids Surf A: Physicochem Eng Asp*, 2004, 249(1/2/3): 115-118.
- [30] Deng Tong, Dai Yujie, Wang Jing. A new kind of dispersion-colloidal emulsion aphrons [J]. *Colloids Surf A: Physicochem Eng Asp*, 2005, 266(1/2/3): 97-105.
- [31] LaMer V K, Dinegar R H. Theory, production and mechanism of formation of monodispersed hydrosols [J]. *J Am Chem Soc*, 1950, 72(11): 4847-4854.
- [32] Destrée C, Nagy J B. Mechanism of formation of inorganic and organic nanoparticles from microemulsions [J]. *Advances in Colloid and Interface Science*, 2006, 123/124/125/126: 353-367.
- [33] Geng Fengxia, Zhao Zhigang, Cong Hongtao, et al. An environment-friendly microemulsion approach to a-FeOOH nanorods at room temperature [J]. *Materials Research Bulletin*, 2006, 41: 2238-2243.
- [34] Oleksakova D, Kollar P, Fuzer J, et al. The influence of mechanical milling on structure and soft magnetic properties of NiFe and NiFeMo alloys [J]. *Journal of Magnetism and Magnetic Materials*, 2007, 316(3): e838-e841.
- [35] Landi B J, Cress C D, Evans C M, et al. Thermal oxidation profiling of single-walled carbon nanotubes [J]. *Chem Mater*, 2005, 17(26): 6819-6834.
- [36] Furtado C A, Kim U J, Gutierrez H R, et al. Debundling and dissolution of single-walled carbon nanotubes in amide solvents [J]. *J Am Chem Soc*, 2004, 126(19): 6095-6105.
- [37] Wriedt H, Gokcen N A, Nafziger R H. "Fe-N (Iron-Nitrogen)" *Phase Diagrams of Binary Iron Alloys* [M]. ASM International Materials Park, 1993.
- [38] Raghavan V. The Cr-Fe-N-Ni system (chromium-iron-nitrogen-nickel) [J]. *Journal of Phase Equilibria*, 1997, 18(2): 158-172.
- [39] Swartzendruber L J, Itkin V P, Alcock C B. "Fe-Ni (Iron-Nickel)" *Phase Diagrams of Binary Iron Alloys* [M]. ASM International Materials Park, 1993.
- [40] Wells A F. *Structural Inorganic Chemistry* [M]. Oxford: Clarendon Press, 1975.